

Easy-axis Heisenberg model on the triangular lattice: from supersolid to gapped solid

M. Ulaga,^{1,2} J. Kokalj,^{3,1} T. Tohyama,⁴ and P. Prelovšek¹

¹*Jožef Stefan Institute, SI-1000 Ljubljana, Slovenia*

²*Max Planck Institute for Physics of Complex Systems, Dresden, Germany*

³*Faculty of Civil and Geodetic Engineering, University of Ljubljana, SI-1000 Ljubljana, Slovenia*

⁴*Department of Applied Physics, Tokyo University of Science, Tokyo 125-8585, Japan*

We investigate the easy-axis Heisenberg model on the triangular lattice by numerically studying excitations and the dynamical spin structure factor $S^{\mu\mu}(\mathbf{q}, \omega)$. Results are analyzed within the supersolid scenario, characterized by the translation-symmetry-breaking parameter m_z and the supersolid offdiagonal order parameter m_{\perp} . We find very robust $m_z > 0$ in the whole easy-axis anisotropy regime $\alpha = J_{\perp}/J_z > 0$, even enhanced by the magnetic field $h > 0$, as well as $m_{\perp} > 0$ for intermediate $\alpha < 1$ and $h > 0$. Still, at small $\alpha \lesssim 0.2$, relevant for recent experiments on the magnetic material $\text{K}_2\text{Co}(\text{SeO}_3)_2$, we find at $h = 0$ rather vanishing $m_{\perp} \sim 0$, consistent with the numerical evidence of the finite magnon excitation gap $\Delta_1 \sim 0.25\alpha J$.

Introduction. The antiferromagnetic (AFM) Heisenberg spin-1/2 model on the triangular lattice (TL) has been the origin of several fundamental scenarios since its solution in the Ising limit revealed finite entropy even at $T = 0$ [1]. On the other hand, the isotropic case has been the first candidate for the quantum spin liquid (QSL) [2], while later numerical studies established the ground state (gs) as a symmetry-broken state, breaking translational symmetry with a $\sqrt{3} \times \sqrt{3}$ supercell and spins in 120° alignment [3–6]. The span of easy-axis anisotropies $0 < \alpha = J_{\perp}/J_z < 1$ opens another interesting dimension [7]. Whereas the gs broken translational symmetry persists in the whole intermediate range $0 < \alpha \leq 1$ (representing a spin solid with longitudinal order parameter $m_z > 0$), the most appealing is the scenario of a spin supersolid [8] which requires simultaneously broken rotational in-plane symmetry and finite off-diagonal long-range order (LRO) signalled by $m_{\perp} > 0$. Several numerical studies seem to confirm this possibility for $\alpha < 1$ [9–15], leaving the question of its persistence for small $\alpha \ll 1$.

The challenges revived with recent synthesis and experiments on several novel materials which represent the realization of the easy-axis Heisenberg spin-1/2 model on TL. The most interesting candidate is $\text{K}_2\text{Co}(\text{SeO}_3)_2$ (KCSO) [16] which (due to the convenient value of J_z) allows for various experimental investigations, in particular of thermodynamic quantities and spin excitation spectra via the inelastic neutron scattering (INS), in a wide range of temperatures T and external fields h [17, 18] (see also [19]). Since the material is close to the Ising limit, i.e., with effective $\alpha \sim 0.07$, the central question is whether it is in fact the realization of the spin supersolid. There are also other challenging novel materials, e.g., $\text{Na}_2\text{BaCo}(\text{PO}_4)_2$ [20–23], with $\alpha \sim 0.6$ closer to the isotropic case and $\text{NdTa}_7\text{O}_{19}$ [24] with $\alpha \ll 1$, which has so far experimentally revealed features closer to QSL.

In this Letter, we present the results of numerical finite-size studies of the easy-axis Heisenberg model on TL, which are consistent with the supersolid scenario for

intermediate $0.5 \leq \alpha < 1$, but as well as at finite fields $h > 0$ for the KSCO-relevant regime $\alpha \sim 0.1$. Still at $h \sim 0$ we find for small $\alpha \lesssim 0.2$, besides the robust quasi-elastic peak representing diagonal LRO and finite $m_z > 0$, rather vanishing $m_{\perp} \sim 0$ which is compatible with finite magnon excitation gaps also established numerically. This finding is consistent with our recent general study of thermodynamic properties of the model [25] which were interpreted as a crossover/transition at $\alpha^* \sim 0.3$ to a regime $\alpha < \alpha^*$ characterized by finite excitation gaps.

In the Ising-like regime with $\alpha \ll 1$, it is very instructive to study static and dynamical properties of the spin system, allowing to start the analysis from the extended magnetization plateau $m = 1/3$ at finite $h \sim h_c$ (see also [26]). By decreasing $h < h_c$ our results for the $T = 0$ dynamical spin structure factor (DSSF) $S(\mathbf{q}, \omega)$, calculated on finite systems via exact diagonalization (ED) up to $N = 36$ sites, reveal a gapless magnon mode emerging from $m_{\perp} > 0$, but also squeezed low- ω spectra originating from strongly correlated magnons. Still, on approaching $h \sim 0$ excitations gain a persistent finite magnon gap $\Delta_1 \propto \alpha J$ [25], which we confirm by the density-matrix renormalization group (DMRG) calculation on $N \leq 60$ sites. Moreover, the same conclusion follows also from an effectively reduced model, where the translational symmetry is explicitly broken.

Model. We consider the anisotropic $S = 1/2$ Heisenberg model with the nearest-neighbor (nn) exchange interaction $J_z = J$ and the easy-axis anisotropy $0 < \alpha \leq 1$ on TL in the presence of a longitudinal magnetic field h ,

$$H = J \sum_{\langle ij \rangle} [S_i^z S_j^z + \frac{\alpha}{2} (S_i^+ S_j^- + S_i^- S_j^+)] - h \sum_i S_i^z, \quad (1)$$

where the first sum runs over nn pairs on TL. Note that we further represent h in units J . Our previous study [25] of finite- T properties of the same model on TL, Eq. (1), employing the finite-temperature Lanczos method (FTLM) [27, 28], already pointed out some results now directly relevant for KSCO. In particular, the

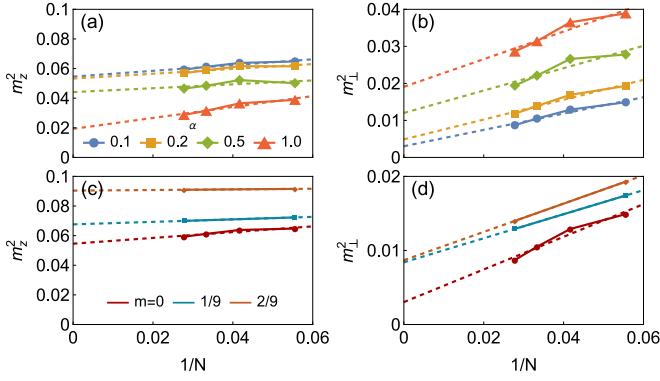


Figure 1. (a) Diagonal LRO moments m_z^2 and (b) the off-diagonal m_\perp^2 vs. $1/N$ for different $\alpha = 0.1 - 1$ and $h = 0$ as extracted from numerical results for $S^{\mu\mu}(\mathbf{q}_K, \omega)$ on TL with $N = 18 - 36$. (c) m_z^2 and (d) m_\perp^2 , again vs. $1/N$, but for $h \geq 0$ and corresponding magnetizations $m \geq 0$.

specific heat $c(T)$ exhibits a pronounced Schottky-like peak at $T^* \sim 0.3\alpha J$ for small $\alpha < \alpha^*$, which is well consistent with the experimentally observed $T^* \sim 1K$ in KSCO [16] and estimated $J \sim 3meV$ and $\alpha = J_\perp/J_z \sim 0.07$ [17, 18]. Related is also large remanent spin entropy in KSCO at $T > T^*$ [16]. Results for the static spin structure factor $S_{\mathbf{q}}^{zz}(T \sim 0)$ [25] also confirm the robust diagonal LRO at $T \sim 0$ consistent with a $\sqrt{3} \times \sqrt{3}$ spin solid.

Let us first consider the $T = 0$ (gs) DSSF $S^{\mu\mu}(\mathbf{q}, \omega) = \langle \psi_0 | S_{-\mathbf{q}}^\mu \delta(\omega - H + E_0) S_{\mathbf{q}}^\mu | \psi_0 \rangle$, with respect to the gs $|\psi_0\rangle$ and its energy E_0 (in general for $h \geq 0$), whereby $S_{\mathbf{q}}^\mu = N^{-1/2} \sum_i e^{i\mathbf{q}\cdot\mathbf{R}_i} S_i^\mu$ and $\mu = x, z$. DSSF is calculated numerically via ED, employing the Lanczos technique (see, e.g., Ref. 29), on TL with $N = 18 - 36$ sites with periodic boundary conditions (PBC) for the related discrete \mathbf{q} in the Brillouin zone (BZ). It should be stressed that the application of PBC (as well as finite-size scaling of results) appears crucial for such frustrated systems.

Diagonal and off-diagonal LRO. We first focus on results at $h = 0$, where the gs corresponds to $S_{tot}^z = 0$ and $\mathbf{q}_\Gamma = 0$. The DSSF reveals a well-pronounced low- ω BZ corner mode at $\mathbf{q}_K = (4\pi/3, 0)$ (in r.l.u.), i.e., $S^{zz}(\mathbf{q}_K, \omega) \sim A^{zz} \delta(\omega - \Delta_{0K})$ (excitations within the same S_{tot}^z sector) and $S^{xx}(\mathbf{q}_K, \omega) \sim A^{xx} \delta(\omega - \Delta_{1K})$ (representing transitions with $\Delta S_{tot}^z = \pm 1$), respectively. The effective LRO parameters are then extracted as $m_z^2 = A^{zz}/N$ and $m_\perp^2 = A^{xx}/N$, following their asymptotic behavior for $N \rightarrow \infty$. Results, obtained for a wide range of $\alpha = 0.1 - 1$ and for systems with $N = 18, 24, 30, 36$ sites, are presented in Fig. 1(a,b). It should be acknowledged that finite-size scaling of results (presented vs. $1/N$) is not (expected to be) perfect since considered systems with PBC have rather different shapes, although they are all chosen to include relevant \mathbf{q}_K in the BZ.

Results in Fig. 1(a,b) reveal qualitative differences be-

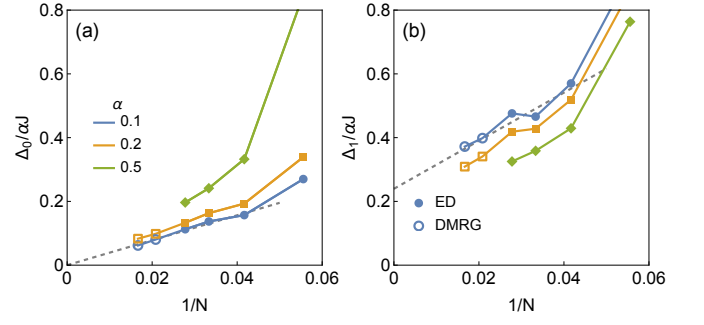


Figure 2. The normalized excitation gaps vs. $1/N$, obtained from ED (for $N \leq 36$) and DMRG (for $N > 36$): (a) $\Delta S_{tot}^z = 0$ “singlet” gap $\Delta_0/(\alpha J)$, (b) $\Delta S_{tot}^z = \pm 1$ magnon gap $\Delta_1/(\alpha J)$, together with simple $N \rightarrow \infty$ extrapolations for $\alpha = 0.1$.

tween nearly isotropic $\alpha \sim 1$ and the Ising-like $\alpha < \alpha^* \sim 0.3$ regimes [25]. In the isotropic case $\alpha = 1$, the extrapolation for $N \rightarrow \infty$ yields consistent (and numerically nontrivial) $m_\perp = m_z \sim 0.14$. It is worth noting that the obtained value is well below, even for modest $N = 18$, apparently accepted value $m_z \sim 0.2$ [5, 6], but closer to some later results [13]. By reducing $\alpha < 1$ we establish increasing m_z and decreasing m_\perp . While for $\alpha \leq 0.2$ our results confirm the saturation of $m_z^2 \sim 0.06$ [13, 26], the asymptotic off-diagonal value is very small $m_\perp^2 \ll 0.01$, essentially below the reliable extrapolation. Moreover, the observed scaling $m_\perp^2 \propto 1/N$ implies that A^{xx} is rather N -independent, pointing to a finite magnon gap $\Delta_1 > 0$, analyzed in more detail below.

Excitation gaps. A complementary message arises from the consideration of the lowest spin excitations. For sizes $N \leq 36$ we calculate them via ED directly or extract them from corresponding DSSF. Moreover, we employ here also the DMRG approach [30], which allows to establish gs and first excited states in different S_{tot}^z sector, for much larger lattices $N \leq 60$, again with PBC. The details on the method and corresponding results are presented in Supp. [31]. In Fig. 2(a) we show the evolution of the “singlet” gap $\Delta_0 = E_{\mathbf{q}_K}^0 - E_0^0$ vs. $1/N$ from ED (E_0^0 corresponding to $\mathbf{q}_\Gamma = 0$), combined with the DMRG results for $\alpha \leq 0.2$ (where values are well converged). The normalized $\Delta_0/(\alpha J)$ in Fig. 2(a) indicates a quantitative similarity for all $\alpha \leq 1$, with (linearly in $1/N$) vanishing $\Delta_0 \rightarrow 0$ for $N \rightarrow \infty$. This is consistent with diagonal LRO at $N \rightarrow \infty$ with emergent $m_z > 0$ and a $\sqrt{3} \times \sqrt{3}$ supercell.

However, this is not the case for Δ_1 , representing the $\Delta S_{tot}^z = \pm 1$ “magnon” gaps, extracted from ED results as $\Delta_1 = E_{\mathbf{q}_K}^1 - E_0^0$. We also note that $\Delta_{1K} = E_{\mathbf{q}_K}^1 - E_0^0 \sim \Delta_1 + \Delta_0$, as relevant for DSSF shown further on, should be the same in the limit $\Delta_0 \rightarrow 0$. In Fig. 2(b) we show $\Delta_1/(\alpha J)$ vs. $1/N$, as obtained via ED and DMRG. At least for $\alpha = 0.5$, Δ_1 decreases with N , presumably consistent with $m_\perp > 0$. On the other hand, for $\alpha \leq 0.2$, re-

sults support finite asymptotic $\Delta_1 \sim 0.25\alpha J$ (somewhat below the result in [25]), consistent with the saturation of A^{xx} and vanishing m_\perp in Fig. 1(b).

Finite fields $h > 0$. The question of the supersolid can be extended to finite fields $h > 0$ and corresponding gs magnetizations $m = 2S_{tot}^z/N > 0$, as directly relevant for experiments on KSCO [17, 18]. In the regime of small $\alpha < \alpha^*$ there is well pronounced $m = 1/3$ plateau [25, 26, 32], with gs $S_{tot}^z = N/6$. For $\alpha \ll 1$ the plateau appears at $h > h_c \sim 1.5\alpha J$. We perform the calculation of $S^{\mu\mu}(\mathbf{q}, \omega)$ for $m > 0$ by choosing proper $h > 0$, and we repeat the analysis of m_z and m_\perp for $h < h_c$, i.e., $m < 1/3$. Since the same (commensurate) $m > 0$ are allowed only in some lattices, we restrict in Fig. 1(c,d) results to $N = 18, 36$ systems (and $\alpha = 0.1$). We note that with increasing $m \rightarrow 1/3$ diagonal m_z^2 is even increasing, i.e., for $\alpha \ll 1$ towards the classical value $m_z^2 \sim 1/12$. At the same time, the $0 < m < 1/3$ results indicate finite $m_\perp > 0$ when extrapolated to $N \rightarrow \infty$, clearly in contrast to the $m = 0$ case. It is also remarkable that extracted m_\perp (for $m > 0$) are essentially α independent (not presented) for $\alpha \leq 0.2$.

The persistence of magnon gap $\Delta_1 > 0$ has implications for the $T = 0$ magnetization curve $m(h)$, in particular to the variation for $h \rightarrow 0$. ED and DMRG results are summarized in [31], implying quite universal dependence $m = m(h/\alpha)$ for $\alpha \leq 0.2$, however, plateaued at $m = 0$ for $h < \Delta_1$.

Effective model. The observation that for $\alpha \ll 1$ the diagonal LRO $m_z^2 \sim 1/12$ in the whole range $m < 1/3$, gives the justification to consider a reduced spin model, where in Eq. (1) we explicitly break the translational symmetry and fix spins on one sublattice to $S_i^z = -1/2$. This gives an anisotropic $\alpha \ll 1$ model, still Eq. (1), but now effectively on a honeycomb lattice (HL) and with fields $\tilde{h} = h + 3J/2$. Such a model remains nontrivial due to strong correlations (at $\alpha \ll 1$) between remaining spins. But at least it allows numerical consideration of larger lattices, in particular, a more detailed evolution starting from the $m = -1/3 + 2\tilde{m}/3$ (TL) plateau, \tilde{m} representing the effective magnetization in HL.

The model at $\tilde{m} \lesssim 1$, just below the plateau $m \lesssim 1/3$, is also solvable using magnon excitations with the dispersion (in r.l.u. of TL),

$$\omega_{\mathbf{q}}^\pm = \frac{\alpha J}{2} [3 \pm |f_{\mathbf{q}}|], \quad f_{\mathbf{q}} = e^{iq_x} + 2e^{-\frac{i}{2}q_x} \cos\left(\frac{\sqrt{3}}{2}q_y\right), \quad (2)$$

Excitations have two branches, with a Dirac-like point $\omega_{\mathbf{q}_K}^+ = \omega_{\mathbf{q}_K}^-$ along the $\Gamma - M$ line (at the corner \bar{K} of the HL BZ, Fig. 3(a)), gapless excitations $\omega_{\mathbf{q}}^- \propto q^2$, and $\omega_{\mathbf{q}}^- \propto \tilde{q}^2$, $\tilde{\mathbf{q}} = \mathbf{q} - \mathbf{q}_K$. Such dispersion should well represent the spin-excitation spectra of the full model at $h \sim h_c$ as well also experimental INS results in KSCO close to $h \lesssim h_c$ [17].

Still, it is challenging to determine the evolution of low-spin excitation in the effective model, when increasing

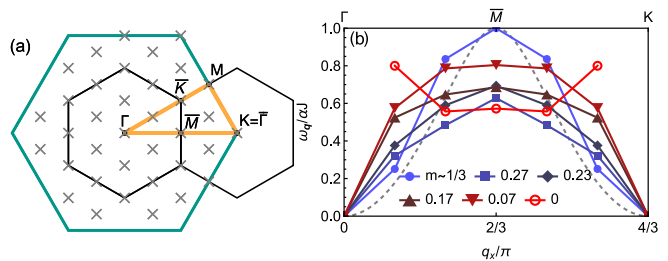


Figure 3. (a) The Brillouin zone for TL (green) and the reduced Brillouin zone for the effective model on HL (black) with marked high-symmetry points, together with discrete \mathbf{q} in the BZ for TL on $N = 36$ sites, (b) Lowest spin excitations $\omega_{\mathbf{q}}/(\alpha J)$ for different m within the reduced model, as calculated numerically for $\alpha = 0.1$ on TL with $N = 60$ sites.

$\tilde{m} \rightarrow 1/2$, i.e, reducing $m \rightarrow 0$. We present in Fig. 3(c) the numerical result for the dispersion of the lowest excitations $\omega_{\mathbf{q}} = E_{\mathbf{q}} - E_0$ for different effective m , as obtained now with ED on the largest system corresponding to TL on $N = 60$ sites. While for $m \sim 1/3$ results agree with the analytical $\omega_{\mathbf{q}}^-$, Eq. (2), the dispersion squeezes (relative to $m \sim 1/3$) as well as becomes supersolid-like (linear) for small $q, \tilde{q} \rightarrow 0$ with decreasing m . Still, on approaching $m \sim 0$ there is evident qualitative change and results in Fig. 3(b) for $m = 0$ are more consistent with a gapped spectra where again $\omega_{\mathbf{q} \neq 0} > \alpha J/2$ [25].

Dynamical spin response. Let us turn to more complete results for the gs $S^{\mu\mu}(\mathbf{q}, \omega)$, focusing on the Ising-like regime. For $\alpha \ll 1$ $\mu\mu$ polarizations can be qualitatively different and partly complementary, since zz response conserves S_{tot}^z , while xx component reflects $\Delta S_{tot}^z = \pm 1$ transitions. INS experiments measure the spin polarization perpendicular to in-plane \mathbf{q} , therefore we show the corresponding $S^\perp(\mathbf{q}, \omega) = S^{zz}(\mathbf{q}, \omega) + S^{xx}(\mathbf{q}, \omega)$. We present results obtained via ED on the largest TL with $N = 36$ sites, which has rotational symmetry and contains the most relevant \mathbf{q} , in particular, BZ boundary \mathbf{q}_K and \mathbf{q}_M . Still, finite-size limitations (also due to $T = 0$ restriction) remain visible both in \mathbf{q} as well in ω resolution.

We present DSSF without the very strong quasielastic peak at $\omega = \Delta_0$, dominating $S^{zz}(\mathbf{q}_K, \omega)$ and consequently the whole DSSF. Let us first comment on $S^\perp(\mathbf{q}, \omega)$ spectra for $h = 0$ ($S_{tot}^z = 0$). Besides the most interesting dynamical regime $\omega < 3\alpha J$ (discussed in detail further), there are also well-visible nearly dispersionless excitations at $\omega \sim J$ and $\omega \sim 2J$ (see Supp. [31]). These are also present in the INS results for KSCO [18] and emerge (nearly) entirely from $S^{xx}(\mathbf{q}, \omega)$, representing spin flips with $\Delta S_{tot}^z = \pm 1$ in local Ising-like environment $S_{loc}^z = n$, leading to $\omega_{\mathbf{q}} \sim nJ$.

More challenging is the $\omega < \alpha J$ regime and its evolution with the field. The summary of INS-relevant $S^\perp(\mathbf{q}, \omega)$, as it develops in the sub-plateau regime $0 \leq m < 1/3$, is presented in Fig. 4 for fixed $\alpha = 0.1$ and

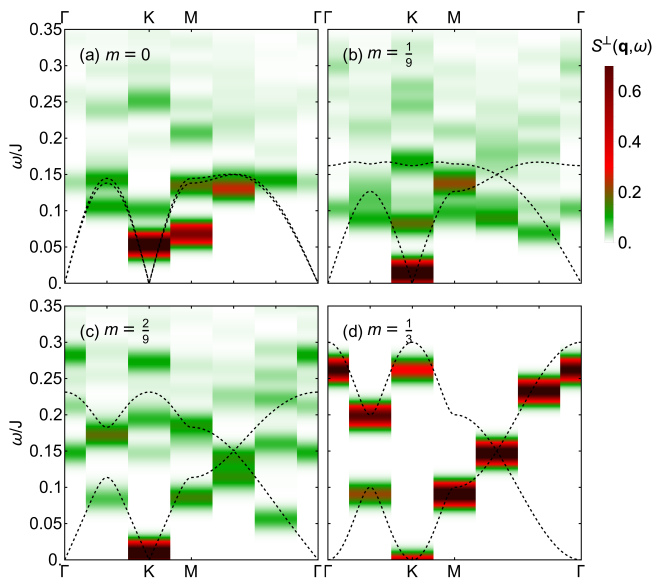


Figure 4. Low- ω regime of the gs DSSF $S^\perp(\mathbf{q}, \omega)$ for $\alpha = 0.1$ and various magnetizations $0 \leq m \lesssim 1/3$ obtained on TL with $N = 36$ sites. Dashed black lines denote the LSW approximation dispersion for $m < 1/3$ and the analytical result for the effective model at $m = 1/3, h \sim h_c$.

for \mathbf{q} along the $\Gamma - K - M - \Gamma$ line in BZ (orange line Fig. 3(a)). Since both \mathbf{q} and ω spectra (at $T = 0$) are discrete, results are represented as broadened for convenience. We start the interpretation with the simplest case, i.e., at the onset of the $m = 1/3$ plateau at $h \lesssim h_c$ in Fig. 4(d). The magnon dispersion here closely follows the analytical expression, Eq. 2, with both lower and upper branches $\omega_{\mathbf{q}}^\pm$ being sharp and well visible, with the main contribution from $S^{xx}(\mathbf{q}, \omega)$.

The evolution with decreasing but finite $0 < m < 1/3$ in Fig. 4(c,b) reveals several generic features: (a) Spectra are less coherent, although with rather well-pronounced lower edges. (b) Consistent with the concept of supersolid and $m_\perp > 0$, the spectra are (nearly) gapless at \mathbf{q}_K , whereby the main contribution emerges from the S^{xx} component. (c) The whole spectra still partly reflect two branches, but are effectively squeezed in ω relative to the $m \sim 1/3$ case. (d) A pronounced dynamical response at \mathbf{q}_M , originating from $S^{zz}(\mathbf{q}, \omega)$, moves down in ω with decreasing m and becomes subdominant compared to the soft \mathbf{q}_K peak in $S^{xx}(\mathbf{q}, \omega)$. While certain features discussed above remain even for the most interesting $m = 0$ in Fig. 4(a), there are some essential differences: (a) The lowest $q \neq 0$ and also the most pronounced excitation emerging from $S^{xx}(\mathbf{q}_K, \omega)$ is now gapped, consistent with $\Delta_{1K} \propto \alpha J$ in Fig. 2b, (b) there is also well-pronounced low- ω excitation at \mathbf{q}_M emerging from $S^{zz}(\mathbf{q}, \omega)$, consistent with INS experiment on KSCO [17] and reminiscent of the roton-like minimum in the isotropic TL [33, 34].

Linear spin-wave theory. It is instructive to consider

the linear spin wave (LSW) approximation for the full model, as also partly shown in Refs. 17 and 26. LSW at $h = m = 0$ suggests $m_\perp \sim \sqrt{\alpha/2}$ for $\alpha \rightarrow 0$ (see Supp. [31]), decreasing with $h > 0$ and vanishing at $h > h_c$. For $m > 0$ this qualitatively (but not quantitatively) agrees with the numerical result in Fig. 1(b), but clearly disagrees with vanishing $m_\perp \sim 0$ at $h \rightarrow 0$. Also, for $m \sim 1/3$ and $m = 2/9$ shown in Figs. 4(c,d) the maximal spectral intensity resembles qualitatively the LSW dispersion, while for $m = 1/9$ and $m = 0$, the agreement is much worse, with a much broader numerical spectra and additional pronounced modes at \mathbf{q}_K and \mathbf{q}_M .

Discussion. Our results confirm that at finite $h > 0$, besides even increased longitudinal $m_z > 0$, there is firm evidence for off-diagonal LRO $m_\perp > 0$, consistent with the theoretical [13, 26] and experimental [17, 18] interpretation in terms of the spin supersolid. This is, however, not the case for the most challenging $h \sim 0$ case, where our extrapolated ED results rather indicate (within numerical resolution) nearly vanishing $m_\perp \sim 0$, which is at least in strong disagreement with the LSW approximation (having the largest m_\perp at $h = 0$). This finding is in fact not inconsistent with tiny (and extrapolation-limited) $m_\perp \gtrsim 0$ in previous studies [13] as well as very recent similar conclusions of Refs. 26 and 35. Moreover, the observed $m_\perp^2 \propto 1/N$ is compatible with the non-vanishing magnon excitation gap $\Delta_1 \propto \alpha J$, well visible in ED results for $S^{xx}(\mathbf{q}, \omega)$ and confirmed directly by DMRG results on systems with up to $N \leq 60$ sites. The gap is also reflected in the absence of low excitations in specific heat $c(T < T^*)$ [25]. In this respect, the large anisotropy regime $\alpha \leq 0.2$ [25] could be different from less anisotropic $\alpha \leq 1$, where the spin supersolid appears to be realized even at $h = 0$ [20, 21, 23].

Making contact to experiments on KSCO, and taking into account assumed values for $J \sim 3\text{meV}$ and $\alpha \sim 0.07$, our best DMRG estimate $\Delta_1 \sim 0.25\alpha J$ would yield $\Delta_1 \sim 0.06\text{meV}$, which might be even compatible with recent INS spectra $S^\perp(\mathbf{q}, \omega)$ at $\mathbf{q} \sim \mathbf{q}_K$ [17]. Otherwise, our calculated DSSF overall correspond well to INS results [17], whereby lower branches can be partly captured by the LSW approximation.

We confirm the gap also within a related effective model on HL allowing ED to reach numerically larger systems. It is evident that in this model magnetic excitations for $\alpha \ll 1$ are strongly repulsive whereby the $h = m = 0$ case corresponds to a commensurate filling in HL. So similarities can be found to the gapped magnon excitations in dimerized J_1 - J_2 chains [36–38] or the planar Shastry-Sutherland model [39]. Nevertheless, establishing and understanding the magnon gap and its presumable vanishing with increasing α remains a future challenge.

Acknowledgments. We thank A. Zheludev and A. Zorko for stimulating discussion of recent experimental results. M.U. further acknowledges discussions with Alexander Wietek and Rafael Alvaro Flores Calderon. This work is supported by the program P1-0044 and project J1-50008 of the Slovenian Research Agency. M.U. acknowledges computing time at HPC Vega at the Institute of Information Science in Maribor under project S24O01-28.

-
- [1] G. H. Wannier, Antiferromagnetism: The triangular Ising net, *Phys. Rev.* **79**, 357 (1950).
- [2] P. W. Anderson, Resonating valence bonds: a new kind of insulator?, *Mat. Res. Bull.* **8**, 153 (1973).
- [3] B. Bernu, P. Lecheminant, C. Lhuillier, and L. Pierre, Exact spectra, spin susceptibilities, and order parameter of the quantum Heisenberg antiferromagnet on the triangular lattice, *Phys. Rev. B* **50**, 10048 (1994).
- [4] L. Capriotti, A. E. Trumper, and S. Sorella, Long-range Néel order in the triangular Heisenberg model, *Phys. Rev. Lett.* **82**, 3899 (1999).
- [5] S. R. White and A. L. Chernyshev, Neel order in square and triangular lattice Heisenberg models, *Phys. Rev. Lett.* **99**, 127004 (2007).
- [6] A. L. Chernyshev and M. E. Zhitomirsky, Spin waves in a triangular lattice antiferromagnet: Decays, spectrum renormalization, and singularities, *Phys. Rev. B* **79**, 144416 (2009).
- [7] S. Miyashita and H. Kawamura, Phase transitions of anisotropic Heisenberg antiferromagnets on the triangular lattice, *J. Phys. Soc. Jpn.* **54**, 3385 (1985).
- [8] M. Boninsegni and N. V. Prokof'ev, Colloquium: Supersolids: What and where are they?, *Reviews of Modern Physics* **84**, 759 (2012).
- [9] D. Heidarian and K. Damle, Persistent supersolid phase of hard-core bosons on the triangular lattice, *Phys. Rev. Lett.* **95**, 127206 (2005).
- [10] M. Boninsegni and N. Prokof'ev, Supersolid phase of hard-core bosons on a triangular lattice, *Phys. Rev. Lett.* **95**, 237204 (2005).
- [11] S. Wessel and M. Troyer, Supersolid hard-core bosons on the triangular lattice, *Phys. Rev. Lett.* **95**, 127205 (2005).
- [12] F. Wang, F. Pollmann, and A. Vishwanath, Extended supersolid phase of frustrated hard-core bosons on a triangular lattice, *Phys. Rev. Lett.* **102**, 017203 (2009).
- [13] H. C. Jiang, M. Q. Weng, Z. Y. Weng, D. N. Sheng, and L. Balents, Supersolid order of frustrated hard-core bosons in a triangular lattice system, *Phys. Rev. B* **79**, 020409 (2009).
- [14] D. Yamamoto, G. Marmorini, and I. Danshita, Quantum phase diagram of the triangular-lattice XXZ model in a magnetic field, *Phys. Rev. Lett.* **112**, 127203 (2014).
- [15] D. Sellmann, X.-F. Zhang, and S. Eggert, Phase diagram of the antiferromagnetic XXZ model on the triangular lattice, *Phys. Rev. B* **91**, 081104 (2015).
- [16] R. Zhong, S. Guo, and R. J. Cava, Frustrated magnetism in the layered triangular lattice materials $K_2Co(SeO_3)_2$ and $Rb_2Co(SeO_3)_2$, *Phys. Rev. Materials* **4**, 084406 (2020).
- [17] M. Zhu, V. Romerio, N. Steiger, S. D. Nabi, N. Mu-
rai, S. Ohira-Kawamura, K. Y. Povarov, Y. Skourski, R. Sibille, L. Keller, Z. Yan, S. Gvasaliya, and A. Zheludev, Continuum excitations in a spin-supersolid on a triangular lattice, *Physical Review Letters* **133**, 186704 (2024), 2401.16581.
- [18] T. Chen, A. Ghasemi, J. Zhang, L. Shi, Z. Tagay, L. Chen, E.-S. Choi, M. Jaime, M. Lee, Y. Hao, H. Cao, B. Winn, R. Zhong, X. Xu, N. P. Armitage, R. Cava, and C. Broholm, Phase Diagram and Spectroscopic Evidence of Supersolids in Quantum Ising Magnet $K_2Co(SeO_3)_2$, *arXiv:2402.15869*.
- [19] F. Mila, From RVB to supersolidity: the saga of the Ising-Heisenberg model on the triangular lattice, *Journal Club for Condensed Matter Physics* (2024).
- [20] N. Li, Q. Huang, X. Y. Yue, W. J. Chu, Q. Chen, E. S. Choi, X. Zhao, H. D. Zhou, and X. F. Sun, Possible itinerant excitations and quantum spin state transitions in the effective spin-1/2 triangular-lattice antiferromagnet $Na_2BaCo(PO_4)_2$, *Nat. Comm.* **11**, 1 (2020).
- [21] Y. Gao, Y. C. Fan, H. Li, F. Yang, X. T. Zeng, X. L. Sheng, R. Zhong, Y. Qi, Y. Wan, and W. Li, Spin supersolidity in nearly ideal easy-axis triangular quantum antiferromagnet $Na_2BaCo(PO_4)_2$, *npj Quantum Materials* **7**, 89 (2022).
- [22] J. Xiang, C. Zhang, Y. Gao, W. Schmidt, K. Schmalzl, C. W. Wang, B. Li, N. Xi, X. Y. Liu, H. Jin, G. Li, J. Shen, Z. Chen, Y. Qi, Y. Wan, W. Jin, W. Li, P. Sun, and G. Su, Giant magnetocaloric effect in spin supersolid candidate $Na_2BaCo(PO_4)_2$, *Nature* **625**, 270 (2024).
- [23] Y. Gao, C. Zhang, J. Xiang, D. Yu, X. Lu, P. Sun, W. Jin, G. Su, and W. Li, Spin Supersolid Phase and Double Magnon-Roton Excitations in a Cobalt-based Triangular Lattice, *arXiv:2404.15997*.
- [24] T. Arh, B. Sana, M. Pregelj, P. Khuntia, Z. Jagličić, M. D. Le, P. K. Biswas, P. Manuel, L. Mangin-Thro, A. Ozarowski, and A. Zorko, The Ising triangular-lattice antiferromagnet neodymium heptatantalate as a quantum spin liquid candidate, *Nat. Mater.* **21**, 416 (2022).
- [25] M. Ulaga, J. Kokalj, A. Wietek, A. Zorko, and P. Prelovšek, Finite-temperature properties of the easy-axis Heisenberg model on frustrated lattices, *Phys. Rev. B* **109**, 035110 (2024).
- [26] Y. Xu, J. Hasik, B. Ponsioen, and A. H. Nevidomskyy, Simulating Spin Dynamics of Supersolid States in a Quantum Ising Magnet, *arXiv:2405.05151*.
- [27] J. Jaklič and P. Prelovšek, Lanczos method for the calculation of finite-temperature quantities in correlated systems, *Phys. Rev. B* **49**, 5065 (1994).
- [28] J. Jaklič and P. Prelovšek, Finite-temperature properties of doped antiferromagnets, *Adv. Phys.* **49**, 1 (2000).
- [29] P. Prelovšek and J. Bonča, Ground state and finite temperature lanczos methods, in *Strongly Correlated Systems - Numerical Methods*, edited by A. Avella and F. Mancini (Springer, Berlin, 2013).
- [30] S. R. White, Density-matrix algorithms for quantum renormalization groups, *Phys. Rev. B* **48**, 10345 (1993).
- [31] See Supplemental Material for more details on the DMRG method and extracted magnetization curve, on the dynamical spin structure factor, as well as on the analysis within the linear spin-wave approximation.
- [32] A. Honecker, J. Schulenburg, and J. Richter, Magnetization plateaus in frustrated antiferromagnetic quantum spin models, *J. Phys. Condens. Matter* **16**, S749 (2004).
- [33] W. Zheng, J. O. Fjærestad, R. R. P. Singh, R. H. McKen-

- zie, and R. Coldea, Excitation spectra of the spin- $\frac{1}{2}$ triangular-lattice heisenberg antiferromagnet, [Phys. Rev. B **74**, 224420 \(2006\)](#).
- [34] F. Ferrari and F. Becca, Dynamical structure factor of the $J_1 - J_2$ Heisenberg model on the triangular lattice: Magnons, spinons, and gauge fields, [Phys. Rev. X **9**, 031026 \(2019\)](#).
- [35] C. A. Gallegos, S. Jiang, S. R. White, and A. L. Chernyshev, Phase diagram of the easy-axis triangular-lattice $J_1 - J_2$ model, [arXiv:2412.03648](#).
- [36] C. K. Majumdar and D. Ghosh, On next-nearest-neighbor interaction in linear chain., [J. Math. Phys. **10**, 1388 \(1969\)](#).
- [37] G. S. Uhrig and H. J. Schulz, Magnetic excitation spectrum of dimerized antiferromagnetic chains, [Phys. Rev. B **54**, R9624 \(1996\)](#).
- [38] J. P. Pouget, P. Foury-Leylekian, S. Petit, B. Hennion, C. Coulon, and C. Bourbonnais, Inelastic neutron scattering investigation of magnetostructural excitations in the spin-peierls organic system $(\text{TMTTF})_2\text{PF}_6$, [Phys. Rev. B **96**, 035127 \(2017\)](#).
- [39] B. S. Shastry and B. Sutherland, Excitation spectrum of a dimerized next-neighbor antiferromagnetic chain, [Phys. Rev. Lett. **47**, 964 \(1981\)](#).
- [40] S. Toth and B. Lake, Linear spin wave theory for single-q incommensurate magnetic structures, [J. Phys. Condens. Matter **27**, 166002 \(2015\)](#).

Supplemental Material: Easy-axis Heisenberg model on the triangular lattice: from supersolid to gapped solid.

M. Ulaga^{1,2}, J. Kokalj^{3,1}, T. Tohyama⁴, and P. Prelovšek¹

¹*J. Stefan Institute, SI-1000 Ljubljana, Slovenia*

²*Max Planck Institute for Physics of Complex Systems, Dresden, Germany*

³*Faculty of Civil and Geodetic Engineering, University of Ljubljana, SI-1000 Ljubljana, Slovenia*

⁴*Department of Applied Physics, Tokyo University of Science, Tokyo 125-8585, Japan*

In the Supplemental Material we present more details on the DMRG method and extracted magnetization curve, on the dynamical spin structure factor, as well as on the analysis within the linear spin-wave approximation.

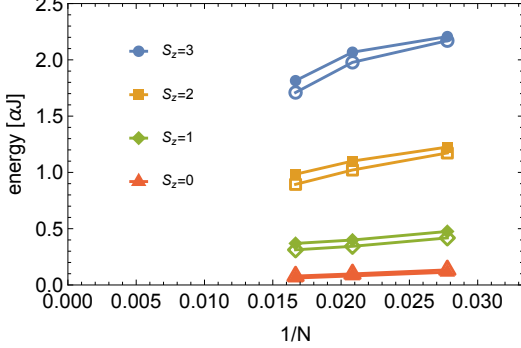


Figure S1. Lowest excitation energies $E_k^0/(\alpha J)$ for different $k = S_{tot}^z/L$ sectors, relative to the gs E_0^0 , as calculated via DMRG for different systems with $N = 36 - 60$ sites, for two anisotropies: $\alpha = 0.1$ (full symbols), and $\alpha = 0.2$ (empty).

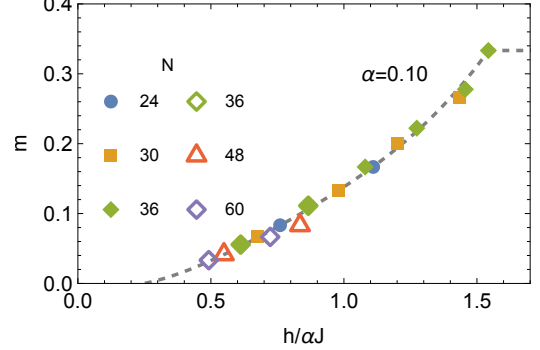


Figure S2. Magnetization m vs. renormalized magnetic field h/α at $T = 0$ and $\alpha = 0.1$, as calculated from ED and DMRG gs energies in each S_{tot}^z sector. The line represents a simple interpolation targeted at $h \rightarrow 0$.

DMRG method and results.

In the DMRG calculations, we use $N = 6 \times 6$, 6×8 , and 6×10 clusters with PBC and perform a snake-type sweeping procedure. The bond dimension is taken to be $\chi = 8000$, leading to a truncation error less than 2×10^{-5} for $\alpha = 0.1$ and $\alpha = 0.2$. This χ gives good convergence of the energy: for example, a relative energy difference between $\chi = 5000$ and 8000 is less than 0.3% for $\alpha = 0.2$ at $N = 60$. On the other hand, the difference is more than 1% for $\alpha = 0.5$. A decrease in accuracy for large α is due to the increase of transverse exchange terms proportional to α , which inevitably induces effective long-range hopping in the sweeping process of DMRG under PBC. Therefore, we restrict the DMRG results only for $\alpha = 0.1, 0.2$. For larger α and N with PBC, we need larger χ , which will be a future work.

Magnetization curve.

With known gs energies E_k^0 within each spin sector $k = S_{tot}^z/N = [-N/2, N/2]$ we can establish the $T = 0$ magnetization curve $m(h)$ by using here the interpolation $h = (E_{k+1}^0 - E_{k-1}^0)/2$, whereby the related magnetization is $m = kN/2$. We are interested in the regime below the

plateau $m \leq 1/3$. Besides ED results for $N \leq 36$ available for all $k \leq N/2$ we take into account also DMRG results, presented in Fig. S1, which are crucial in the most delicate regime $h \rightarrow 0$. In Fig. S2 we present the normalized magnetization curve $m(h/\alpha)$ for chosen $\alpha = 0.1$, which is (within our finite-size restrictions) nearly identical to the result for $\alpha = 0.2$. While such curves have been studied and presented for the isotropic case $\alpha \sim 1$ [32], mostly discussed in relation to the existence and vicinity of the plateau regime, here we focus on the weak fields $h \rightarrow 0$. It is evident that finite $\Delta_1 > 0$ has qualitative consequences and should lead finally to a plateau with vanishing $m(h < \Delta_1) = 0$, and this tendency is observable in Fig. S2. However, It should be pointed out that (compared to experiment, e.g. [17]) the variation at $h \rightarrow 0$ is very sensitive to temperature T , requiring at least $T \leq \Delta_1$.

Dynamical spin structure factor.

Fig. S3 shows DSSF at $h = m = 0$, here separately for $S^{zz}(\mathbf{q}, \omega)$ and $S^{xx}(\mathbf{q}, \omega)$, for chosen $\alpha = 0.1$ and \mathbf{q} along the $\Gamma - K - M - \Gamma$ line in the BZ. Results, as obtained for discrete \mathbf{q} , here via ED for TL with $N = 36$ sites, are extended in \mathbf{q} to improve visibility. The

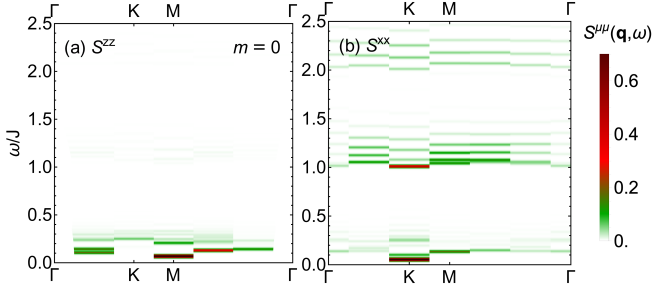


Figure S3. $T = 0$ DSSF (a) $S^{zz}(\mathbf{q}, \omega)$ and (b) $S^{xx}(\mathbf{q}, \omega)$, as obtained for $h = 0$ and $\alpha = 0.1$ on TL with $N = 36$ sites, presented in a broad $\omega/J \gg 1$ range. Spectra are artificially broadened with broadening $\eta = 0.01$.

lowest excitations are represented in both components, being displayed and discussed in the main text. On the other hand, higher energy branches of nearly dispersionless magnetic excitations appearing at $\omega \sim nJ$ are well pronounced only in $S^{xx}(\mathbf{q}, \omega)$. They emerge from spin flips with $\Delta S_{tot}^z = \pm 1$ in local Ising-like spin nearest-neighbor environments $S_{loc}^z = n$.

Analysis within the linear spin-wave approximation.

The LSW approximation starts from classical ground state, which in the discussed regime has three sublattices, with spin on one sublattice pointing down, while the other two pointing up, but at certain angle ϑ (and symmetrically) from the z direction (the planar "Y" state). The energy of such a state can be expressed as

$$\frac{E(\vartheta)}{N} = -S^2 J(2 \cos \vartheta - \cos^2 \vartheta + \alpha \sin^2 \vartheta) - \frac{hS}{3}(2 \cos \vartheta - 1), \quad (\text{S1})$$

with the ground state ϑ corresponding to the minimum of $E(\vartheta)$. With decreasing α and increasing h the angle ϑ is becoming smaller, which decreases $m_{\perp} = S \sin \vartheta$ and can be expressed analytically as

$$m_{\perp}/S = \sqrt{1 - [(1 + h/(3SJ))/(1 + \alpha)]^2}, \quad (\text{S2})$$

with $S = 1/2$, i.e., $m_{\perp} \sim \sqrt{\alpha/2 - h/(3J)}$ for $\alpha \ll 1$ relevant here. As $\alpha \rightarrow 0$, the classical result gives decreasing $m_{\perp} \sim \sqrt{\alpha/2}$.

Once the classical ground state is determined, the LSW dispersions are calculated by following Ref. 40 and shown

in the main text. We note that at $m \sim 1/3$ the full model LSW approximations give slightly lower energies at the upper edge of the second branch, than the effective HL model and the analytical result shown in Fig. 4d in the main text. The LSW results shown in the main text in Figs. 4(b,c) are calculated at the magnetic fields h that give the corresponding magnetizations m in the numerical ED calculation. We also find that in the calculated small α regime the LSW lower branch dispersion width

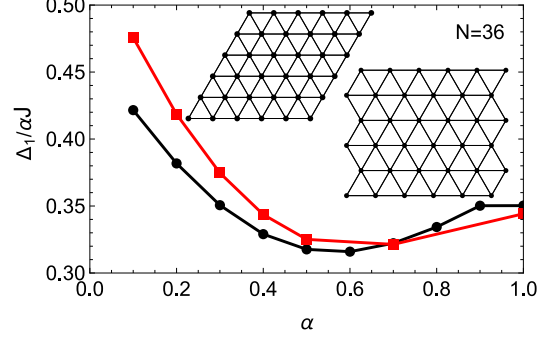


Figure S4. The magnetic gap as a function of anisotropy on inequivalent $N = 36$ clusters: the rhomb (red) and square (black).

and magnon velocity v are proportional to α at $h = 0$, while v at finite fields can be within LSW quite well approximated with $v(\alpha, h) \sim \alpha m_{\perp}(\alpha, h)/m_{\perp}(\alpha, h = 0)$.

Cluster shape analysis.

Some dependence of the cluster shape chosen for the $N = 36$ system is summarized in Fig. S4. The rhombic cluster selected for the analysis in the rest of the manuscript is fully compatible with the infinite lattice symmetry, including 6-fold rotational symmetry, and possesses 7 inequivalent \mathbf{q} points. Alternatively, one can choose a "square-ish" cluster with lesser symmetry and more, 15, inequivalent \mathbf{q} points. We note that the magnetic gaps Δ_1 differ by $\sim 10\%$ between the two clusters with the gap being slightly smaller on the square cluster at small α , but generally follow the same behavior. The shape influence on nonmagnetic gaps Δ_0 (not shown) is minimal.